Electronic Supplementary Information (ESI)

Tunable synaptic behaviors of solution-processed InGaO film for artificial visual system

Pengsheng Li‡[a], Honglin Song‡[b], Zixu Sa‡[a], Fengjing Liu[a], Mingxu Wang[a], Guangcan Wang[a], Junchen Wan[a], Zeqi Zang[a], Jie Jiang*[b] and Zai-xing Yang*[a]*

[a] School of Physics, Shandong University, Jinan 2510100, China.

[b] Hunan Key Laboratory of Nanophotonics and Devices, School of Physics and Electronics, Central South University, Changsha 410082, China.

*Address Correspondence to F. Liu (liufj@sdu.edu.cn), J. Jiang (jiangjie@csu.edu.cn) and Z.-x. Yang (zaixyang@sdu.edu.cn).

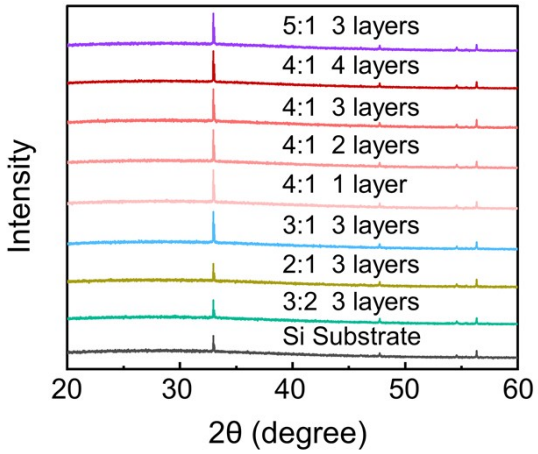

Fig. S1 XRD of InGaO films under different In/Ga ratio and thickness.

As shown in X-ray diffraction of Fig. S1, only peaks of substrates are observed, indicating the amorphous nature of as-prepared InGaO films. This result is in line with the previous literatures[1,2].

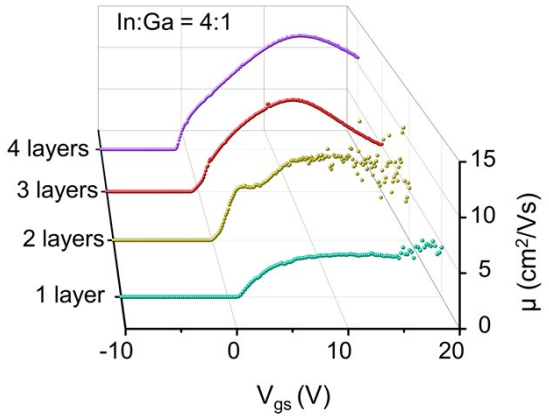

Fig. S2 The field-effect mobilities of as-prepared InGaO films with different film thickness.

As we known, the field-effect mobility (μ) can be obtained from the followed formula[3]:

$$\mu = 2L \cdot (\partial I_{ds}^{1/2}/\partial V_{gs})^2/WC_{ox}$$

where L is the channel length, I_{ds} is the drain current, V_{gs} is the gate voltage, W is the channel width and C_{ox} is the gate capacitance. As shown in Fig. S2, with the L of 10 μm, W of 1000 μm, and C_{ox} of 0.69 fF/μm^2, the peak field-effect mobility increases from 4.76 to 8.26 and 10.05 and 13.34 cm^2/Vs with the increase of film thickness, benefiting from the increase in carrier concentration due to the increase in the number of oxygen vacancies[4,5].

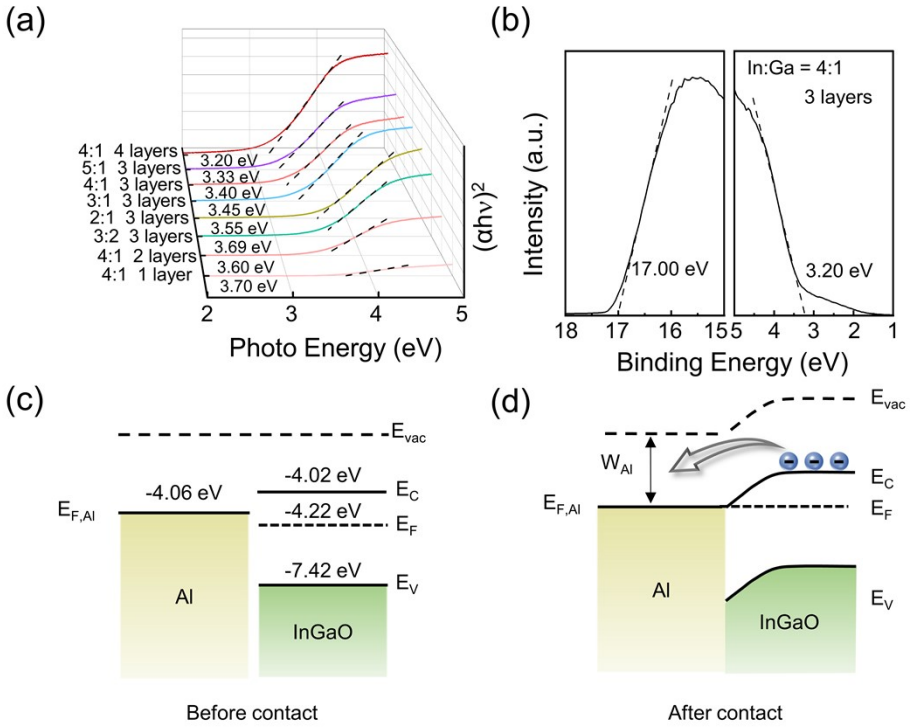

Fig. R3 (a) UV-Vis of InGaO films under different In/Ga ratio and thickness. (b) UPS spectra of the InGaO film. (c, d) Band diagrams of InGaO and metal Al before and after contact.

The bandgap structures of InGaO films are determined by UV-Vis and ultraviolet photoelectron spectroscopy (UPS), as shown in Fig. S3. As shown in UV-Vis of Fig. S3(a), when the thickness

is 3 layers, the bandgaps of InGaO films gradually decrease with the increase of In/Ga ratio, showing values of 3.69, 3.55, 3.45, 3.40, 3.30 eV. When the ratio of In/Ga is constant, the bandgaps of InGaO films gradually decrease with the increase of thickness, showing values of 3.70, 3.60, 3.40, 3.20 eV. From UPS of Fig. S3(b), the cutoff energy boundary (E_{cutoff}) and onset boundary (E_{onset}) of the InGaO film are 17.00 and 3.20 eV, respectively. The valence band (E_V) and Fermi level (E_F) are calculated as - 7.42 and - 4.22 eV, respectively, according to the formula of E_V = - [21.22 - (E_{cutoff} - E_{onset})] and E_F = - ($|E_V|$ - E_{onset}), respectively. With the bandgap of 3.4 eV, the conduction band (E_C) of the InGaO film is calculated as - 4.02 eV, as shown in Fig. S3(c). As shown in Fig. S3(d), metal Al has a work function of 4.06 eV, and when it comes into contact with InGaO film, ohmic contact will be formed.[6,7].

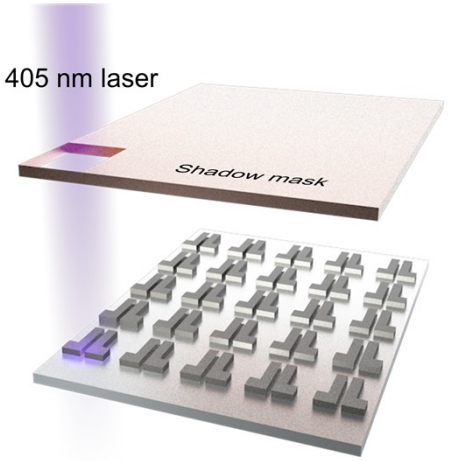

Fig. S4 Schematic of the imaging system.

By individually testing different devices, the corresponding imaging results are obtained. For preventing the laser to affect other devices, a shadow mask is used to shield the other devices, as shown in Fig. S4. During the testing process, the current values are recorded at 0 s, 10 s, and 30 s after illumination. When changing the number of light pulses, positive V_{gs} pulses needs to be applied before testing to reset the device to its initial state, and then the test can be conducted.

References

1 W. Huang, P. H. Chien, K. McMillen, S. Patel, J. Tedesco, L. Zeng, S. Mukherjee, B. Wang, Y. Chen, G. Wang, Y. Wang, Y. Gao, M. J. Bedzyk, D. M. DeLongchamp, Y. Y. Hu, J. E. Medvedeva, T. J. Marks, A. Facchetti, *Proc Natl Acad Sci U S A*, 2020, **117**, 18231-18239.

2 J. Zhang, Z. Sa, P. Li, Z. Zhai, F. Liu, M. Wang, G. Wang, Y. Yin, Y. Li, W. Mu, Z. Jia, F. Chen, Z. x. Yang, *Adv. Opt. Mater.*, 2024, **12**, 2302665.

3 P. J. Jeon, J. S. Kim, J. Y. Lim, Y. Cho, A. Pezeshki, H. S. Lee, S. Yu, S. W. Min, S. Im, *ACS Appl Mater Interfaces*, 2015, **7**, 22333-40.

4 R. Tseng, S.-T. Wang, T. Ahmed, Y.-Y. Pan, S.-C. Chen, C.-C. Shih, W.-W. Tsai, H.-C. Chen, C.-C. Kei, T.-T. Chou, W.-C. Hung, J.-C. Chen, Y.-H. Kuo, C.-L. Lin, W.-Y. Woon, S. S. Liao, D.-H. Lien, *Nat. Commun.*, 2023, **14**, 5243.

5 S.-H. Choi, *IEEE Electron Device Lett.*, 2021, **42**, 168-171.

6 M. Wang, X. Zhuang, F. Liu, Y. Chen, Z. Sa, Y. Yin, Z. Lv, H. Wei, K. Song, B. Cao, Z. X. Yang, *Nano Lett*, 2022, **22**, 9707-9713.

7 J. M. Sun, X. M. Zhuang, Y. B. Fan, S. Guo, Z. C. Cheng, D. Liu, Y. X. Yin, Y. F. Tian, Z. Y. Pang, Z. P. Wei, X. F. Song, L. Liao, F. Chen, J. C. Ho, Z. X. Yang, *Small*, 2021, **17**, 2102323.